EACWE 5
Florence, Italy
19th – 23rd July 2009

Numerical investigation of conductor bundle icing

T. Wagner[1], U. Peil[2], C. Borri[3]

[1] *Technische Universität Carolo-Wilhelmina zu Braunschweig, International Graduate School for Risk Management of Natural Hazards, Beethovenstraße 51, 38106 Braunschweig, Germany, t.wagner@tu-bs.de*

[2] *Technische Universität Carolo-Wilhelmina zu Braunschweig, Institute of Steel Structures, Beethovenstraße 51, 38106 Braunschweig, Germany, u.peil@is.tu-braunschweig.de*

[3] *Università degli Studi di Firenze, Dipartimento di Ingegneria Civile, Via di S. Marta 3, 50139 Firenze, Italy, cborri@dicea.unifi.it*

Keywords: transmission line icing, CFD, particle tracing

ABSTRACT

Aerodynamic instability of cables due to ice accretion is a known phenomenon. Ice accretion on conductor bundles can be investigated by experiments as well as by statistical and numerical models. The whole variety of meteorological conditions and bundle characteristics can hardly be examined purely by experiments. Statistical models can provide information about occurrence frequencies of icing events and static ice loads. But shape and aerodynamic coefficients of an iced cable requires simulation of the icing process itself. Existing numerical models are restricted to single cables due to the assumptions made in the flow calculation. Therefore the simulation scheme presented here allows for particle motion based on the stream occurring around conductor bundles. To overcome this restriction, the Finite Element Method (FEM) with a Reynolds Average Navier-Stokes (RANS) model is used to calculate the incompressible Navier-Stokes equation. A k-ε turbulence model is chosen to address the closure problem of the RANS equations. The stream of air and precipitation droplets are modelled as one-way coupled two-phase flow. Ice accretion and flow field are calculated iteratively to account for geometrical changes of the ice deposit in the flow calculation.

Contact person: T. Wagner, Technische Universität Carolo-Wilhelmina zu Braunschweig,
International Graduate School for Risk Management of Natural Hazards,
Beethovenstraße 51, 38106 Braunschweig, Germany, Phone +49 (0)531 / 391-3369, Fax +49 (0)531 / 391-4592.
E-mail t.wagner@tu-bs.de

1. INTRODUCTION

Atmospheric icing occurs when freezing raindrops, supercooled cloud droplets or snow flakes hit a surface. This phenomenon can cause significant damage to electric power transmission networks, especially in combination with wind. Therefore shape and density of ice forming on cables are of major interest in investigating the risk of failure. Large amplitude oscillations at low frequencies or also twisting due to asymmetrical icing of cables can cause fatigue damages. In extreme events atmospheric icing can cause severe damage on towers and power lines (Bendel & Paton 1981, Jones 1998a). A large number of small-scale failures can cause enormous damage just as well as a single major winter storm event (Llinca et al. 1996, Muhlerin 1998). Examples of such events took place in northern America in 1998 and to a much smaller extent in Germany in 2005, where the devastating power of winter storms left many people without electricity for weeks and caused significant monetary damage (Makkonen 2000, Bundesnetzagentur 2006, Lämpke 2006).

The following three reasons make it seem useful to develop a simulation scheme allowing for particle motion based on the stream occurring around conductor bundles: Firstly, meteorological observations from the 1950s give a first hint that tandem arrangements of cylinders have an effect on the icing process (Diem 1955, Waibel 1956). Secondly, the vulnerability of modern societies to blackouts is growing with the increasing demand of energy and increasing use of capacity. Since public authorities in Germany tend to restrict the construction of new transmission lines, bundled conductors are used increasingly to cope with the rising energy demand (Kießling et al. 2001). Thirdly, available numerical models are restricted to single cables due to the assumptions made in the air flow calculation, for example Lozowski et al. (1983), Makkonen (1984, 1989, 1998), Jones (1998b) and Fu et al. (2004, 2006). A good overview of cable icing models and the mechanism of ice accretion is given by Poots (1996) and Makkonen et al. (2000, 2005).

Modelling atmospheric icing includes a computation of the mass flux of icing particles as well as a determination of the icing conditions:

Icing conditions are defined by the heat balance on the ice surface. Messinger (1953) proposed a basic scheme to investigate heat balances on ice surfaces. The icing condition influences the accretion mass and furthermore the evolving ice density. Three major types of deposit, namely rime, glaze and wet snow lead to significant loads on structures. For glaze ice and wet snow formation the heat balance on the ice surface is very important. It is termed as wet growth, because a liquid layer forms on the ice surface. In contrast to that, rime ice develops in dry growing conditions. The heat transfer within the system can be neglected, because the latent heat of the droplets released during freezing is dissipated without changing the state of the ice and the surface conditions, hence no liquid layer arises.

Computation of the mass flux of icing particles is an important factor in the ice accretion. Shape and to a smaller extent also density of ice evolution is influenced by the characteristics of the particle trajectories. The present work focuses on the mass flux of icing droplets and the formation of the ice front. In a first step, this model is limited to a dry ice growing regime, in other words, only rime ice evolution is considered. With further development the model is to include also wet ice conditions.

2. FLUID DYNAMICS

To calculate air flow around the conductors the finite element software COMSOL Multiphysics and a Reynolds Average Navier-Stokes (RANS) model are used (Comsol 2007). The fluid dynamic calculation is based on the incompressible and isothermal Navier-Stokes equation. It assumes a constant density and a constant temperature throughout the fluid domain. Hence, the conservation of mass becomes

$$\nabla \boldsymbol{u} = 0 \tag{1}$$

where $\boldsymbol{u}$ = velocity vector. Assuming the fluid to be Newtonian and adding the Stokes assumption the stress tensor becomes

$$\tau = \eta\left(\nabla \boldsymbol{u} + (\nabla \boldsymbol{u})^T\right) \tag{2}$$

where η = dynamic viscosity. Therefore the conservation of momentum is

$$\rho\frac{\partial \boldsymbol{u}}{\partial t} + (\rho\nabla \boldsymbol{u})\boldsymbol{u} = -\nabla p + \nabla\left(\eta\left(\nabla \boldsymbol{u} + (\nabla \boldsymbol{u})^T\right)\right) + \boldsymbol{F} \tag{3}$$

with ρ = fluid density, p = pressure and $\boldsymbol{F}$ = force vector acting on the body.

The conservation of energy is independent of the other two conservation equations, because density and temperature are assumed to be constant. Therefore it is not included in the flow calculation (Zienkiewicz et al. 2005).

To solve the closure problem of the RANS equations, a k-ε turbulence model is chosen (Zienkiewicz et al. 2005). In spite of its weakness in the pressure representation on body surfaces the k-ε model was preferred at this stage, because of its tendency to ease convergence. A k-ω turbulence model, known for its superior performance in external flow calculations, might be used in a later stage (Schlichting et al. 2006).

The model introduces the turbulent kinetic energy k and the dissipation rate of turbulence ε as independent variables. The closure problem is then solved using the turbulent viscosity, which is determined by

$$\eta_T = \rho C_\mu \frac{k^2}{\varepsilon} \tag{4}$$

where $C_\mu = 0.09$ is a model constant. The turbulent kinetic energy k is derived from the Reynold stresses, which are expressed by

$$\rho\frac{\partial k}{\partial t} - \nabla\left(\left(\eta + \frac{\eta_T}{\sigma_k}\right)\nabla k\right) + \rho \boldsymbol{U}\cdot\nabla k = \frac{1}{2}\eta_T\left(\nabla \boldsymbol{U} + (\nabla \boldsymbol{U})^T\right)^2 - \rho\varepsilon \tag{5}$$

where $\boldsymbol{U}$ = average velocity field and the model constant $\sigma_k = 1.0$. The corresponding equation for ε can only be determined in a similar way when all terms that have no equivalent term in the equation for k are not included. The equation is then defined as

$$\rho\frac{\partial \varepsilon}{\partial t} - \nabla\left(\left(\eta + \frac{\eta_T}{\sigma_\varepsilon}\right)\nabla \varepsilon\right) + \rho \boldsymbol{U}\cdot\nabla \varepsilon = \frac{1}{2}C_{\varepsilon 1}\frac{\varepsilon}{k}\eta_T\left(\nabla \boldsymbol{U} + (\nabla \boldsymbol{U})^T\right)^2 - \rho C_{\varepsilon 2}\frac{\varepsilon^2}{k} \tag{6}$$

where the model constants are $C_{\varepsilon 1} = 1.44$, $C_{\varepsilon 2} = 1.92$ and $\sigma_\varepsilon = 1.3$. They are a commonly used set of model constants developed by Launder & Sharma and published in Wilcox (1998).

One important assumption made by this turbulence model is, that the equilibrium of turbulence is in boundary layers and therefore formation and dissipation of turbulences are equal. Since this is not always true, the spatial extension of recirculation zones is usually underestimated (Comsol 2007).

The extension of the recirculation zone is expected to have a significant influence on the ice formation process on the downstream cable. Therefore the simulation results can underestimate the influence of the wake on the downstream cable.

2.1 Mesh

The fluid domain is meshed with a free mesh. On the cable or respectively the ice surface a boundary layer mesh is inserted. The depth of the boundary layer mesh is chosen to be 1.5 times the depth of a boundary layer derived by an empirical equation for turbulent flows and flat plates (Anderson 1995).

$$\partial(l) = \frac{0.37l}{Re_l^{1/5}} \tag{7}$$

where l = half of the cable and ice surface length and Re_l is the Reynolds number

$$Re_l = \frac{u_0 l}{\nu} \tag{8}$$

where u_0 = free stream velocity and $\nu =$ kinematical viscosity.

2.2 Boundary Conditions and Model Geometry

In contrast to investigations commonly undertaken in the field of aeroelasticity, the gravity needs to be included in the flow calculation to describe the particle motion correctly. Hence the boundary conditions need to balance the hydrostatic pressure. For this purpose pressure constrains are applied on vertices along the inlet and outlet boundary. At the inlet and outlet boundaries the velocity is set to be equal to the free stream velocity. Also at the remaining external boundaries at top and bottom of the domain the velocity is predefined as free stream velocity.

In order to avoid any effects of the boundary conditions of the flow around the investigated objects the domain is divided in a far and near field. Figure 1 shows the model dimensions, which are chosen to provide enough clearance between the external boundaries and the iced cable. So that even for the largest possible blockage in the flow, the influence of the boundaries on cable and ice body is irrelevant. Cable and ice surface are modelled as a solid wall, where the velocity profile at the cable and ice surface is described by the logarithmic wall function. The presumed extension of the boundary layer has an influence on the achieved results. In k-ε turbulence model this assumption should lead to a boundary layer depth in the range of 30-100 viscous units, whereas a maximum value of 200 is still considered as valid. The model satisfies the condition of 30-100 viscous units apart from a few time steps, where the depth of the boundary layer reached a value of 150 viscous units.

To develop an icing algorithm capable to simulate accretion on a conductor bundle, this investigation focuses on two cables in a tandem arrangement. If the algorithm proves successful for two cables, it can easily be applied to other bundle geometries with more cables. Power transmission lines are also constructed with bundles of three, four or even more cables (Kießling et al. 2001). Further bundle geometries will be investigated in the future.

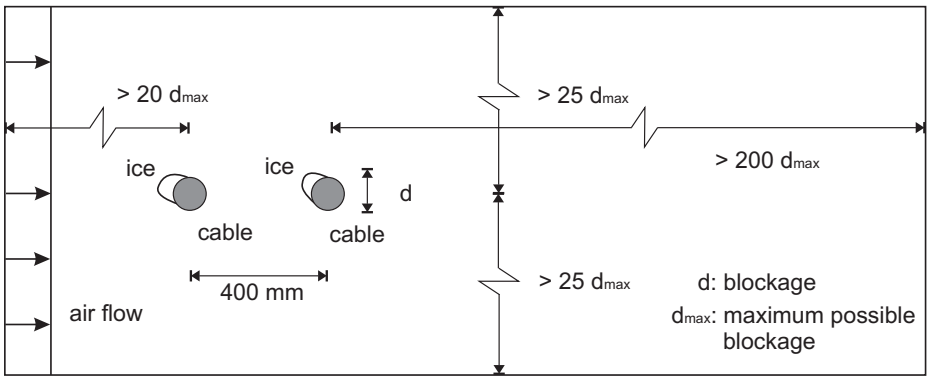

Figure 1: Sketch of the model layout

2.3 Solver

The equation system is solved by a stationary segregated solver algorithm, where the variables are divided in groups. The solver terminates, when the estimated error of all groups is smaller than the given tolerance (Comsol 2007). Here velocity components and pressure compose the first group and the logarithm of turbulent kinetic energy and of turbulent dissipation rate are the second group. The

linear system solver Pardiso is applied to each group (Schenk et al. 2004, 2006). The final error estimate of the results for both groups is e<0.001.

2.4 Solver Verification

The solver used here is a segregated solver. The chosen liner system solver and their settings where examined along a test scheme of the DFG (German Research Foundation) (Schäfer et al. 1996). The benchmark test investigates a 2D flow field passing a cylinder. It gives a feasible range for the five parameters describing the flow field. In a stationary computation the aerodynamic lift and drag coefficient, the length of the recirculation zone, the pressure difference at the stagnation point and the subtending point in the wake are determined. In a transient calculation the maxima of lift and drag coefficient and in addition the Strouhal number are defined. The settings achieved the requirements satisfactorily.

3. PARTICLE TRACING

The mixed stream of air and precipitation particles is described by a one-way coupled two-phase flow. A Lagrangian approach is used to describe the droplet motion in the fluid, meaning that individual particle trajectories are modelled. This approach is used even though it does not provide information about the particle density in the flow field. It is presumed, that there will be a low particle concentration in the flow. Based on this assumption any effect of the particles on the fluid flow is neglected. Therefore, decoupling of the fluid dynamic calculation and the droplet motion description by the Lagrangian method is justified.

Newton's second law is the governing equation describing the particle motion.

$$m\boldsymbol{a}_p = \sum \boldsymbol{F} \tag{9}$$

where m = particle mass, $\boldsymbol{a}_p$ = particle acceleration and $\boldsymbol{F}$ = the sum of drag, buoyancy and gravity acting on the particle. Since the drag force depends on the relative velocity of the droplet and the fluid, the equation becomes numerically expensive. Therefore the following expression is used, which is derived from experiments (Coulson et al. 1991).

$$\boldsymbol{F} = \rho\pi r_p^{\,2} \left(\boldsymbol{u} - \boldsymbol{u}_p\right)^2 \left(1.84\, Re_p^{\,-0.31} + 0.293\, Re_p^{\,0.06}\right)^{3.45} \tag{10}$$

where $\boldsymbol{u}$ = fluid velocity and $\boldsymbol{u}_p$ = particle velocity. The particle Reynolds number is given by

$$Re_p = \frac{\left|u - u_p\right| 2 r_p \rho}{\eta} \tag{11}$$

with r_p = particle radius, ρ = as fluid density and η = dynamic fluid viscosity.

The solver rewrites this second order ordinary differential equation (ODE) into a pair of coupled first order ODE. In each direction it has one equation for velocity and one for location. This system is then solved by a pair of four and five order Runge-Kutta algorithms. The difference between them is used to determine the local error estimate (Comsol 2007). Its tolerance is set to *tol*=1e-12.

Obviously the droplet diameters in natural precipitation are not uniform. They can be described via droplet spectra stating the fractions of the individual droplet diameters (Langmuir & Blodgett 1946). To calculate the motion for every single diameter fraction of particles would be computationally expensive. Fortunately, for the simulation of transmission line icing it is sufficient to deduce the behaviour of the whole spectrum from the motion of a droplet of medium volume diameter (MDV) (Fu 2004).

4. ICING MODEL

The droplet trajectory calculation provides information about the impinging particles, which determine the mass flux on the surface. Once the mass flux is given, the computation of the ice evolution can start. The mass flux can be visualised as a stream tube starting from the undisturbed flow to the surface, limited by the computed droplet trajectories. Within each tube the particles stream from the undisturbed flow towards the surface. The local collection efficiency is the ratio of droplet mass flux in the undisturbed incoming flow to mass flux of droplets impinging on the surface. For in-cloud icing it is given by

$$\beta = \frac{A_0}{A_i} \tag{12}$$

where A_0 = initial trajectory spacing in the undisturbed flow and A_i = trajectory spacing of the impinging particle on the surface.

The developing ice density can be determined by empirical equations. Following the investigation of Fu (2004) the equations derived by Bain & Gayet (1982) where chosen.

$$\rho_i = 110 \cdot R^{0.76} \qquad R \le 10 \tag{13}$$

$$\rho_i = \frac{R}{R + 5.61} \cdot 10^3 \qquad 10 < R \le 60 \tag{14}$$

$$\rho_i = 917 \qquad R > 60 \tag{15}$$

Macklin's Parameter is (Macklin 1962)

$$R = \frac{MDV \cdot u_{p,i}}{2 \cdot T_s} \tag{16}$$

where MDV = medium volume diameter, $u_{p,i}$ = impact speed and T_s = surface temperature. In conjunction with the liquid water content (LCW) in the air the ice accretion ratio is achieved.

$$\chi = \frac{LCW}{\rho_i} \tag{17}$$

The ice front growth along the vector is expressed in

$$\boldsymbol{e}_i = u_{p,0} \cdot \chi \cdot \beta \cdot t_{int} \cdot \boldsymbol{n} \tag{18}$$

where $u_{p,0}$ = particle velocity in the undisturbed flow, t_{int} = time interval of ice evolution with unchanged flow field and $\boldsymbol{n}$ = vector normal to the surface. On the basis of the new ice geometry a new simulation step is started.

4.1 Icing Model Verification

The results of the model are compared with those of single cables presented in the literature. In Figure 2 experimentally and numerically achieved ice shapes are displayed. Only the work done by Fu et al. (2006) is shown here, since the model is already validated by preceding investigation.

The presented model meets the longitudinal extension of the ice body very well for a larger (left) and a smaller (right) cable diameter. The vertical extension deviates in both cases, which is due to the calculation of the particle impinging points on the surface. Each time interval of ice evolution is based only on one charge of particles. Thus, particles impinging furthest to the upper and lower edge in this charge are not necessarily as close to the edge as possible. So that the surface area with no mass flux

at the upper and lower edge is overestimated. If the model would calculate a larger number of trajectories, we would see that some particles actually impinge closer to the edge. Hence, less mass is caught at the upper and lower edge. Comparing the large (left) and smaller (right) cable diameter one can see that this effect increases, when the ice body becomes more streamlined. To overcome this effect, a time interval with several trajectory calculations will be used to estimate the impinging points.

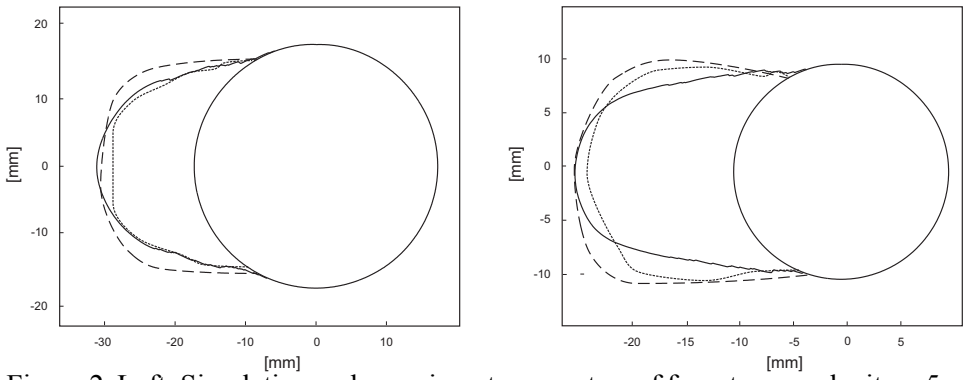

Figure 2. Left: Simulation and experiment parameters of free stream velocity = 5m/s, air temperature = -15°C, MDV = 34µm, cable diameter = 34.9mm; presented model (−), experiment (--) and simulation (···) by Fu (2006). Right: Simulation and experiment parameters of free stream velocity = 5m/s, air temperature = -15°C, MDV = 34µm, cable diameter = 19.5mm; presented model (−), experiment (--) and simulation (···) by Fu (2006). All tests had a duration of 30 minutes and a LCW = 1.2 g/m³.

5. CONCLUSION

The presented model shows the influence of tandem arrangements of cables on icing. As to be expected, one can see in Figure 3 that the upstream cable is catching a larger fraction of the particle flux than the downstream cable in its wake. In general, the shaded area decreases with decreasing deflection of the particle trajectories. It means that larger droplets will deflect less due to higher inertia, presuming a flow pattern with the same Reynolds number. Once the upstream cable gets a more streamlined shape due to the ice accretion, the particle trajectories are deflected to a smaller extent when passing the first cable. Thus the mass flux on the downstream cable increases.

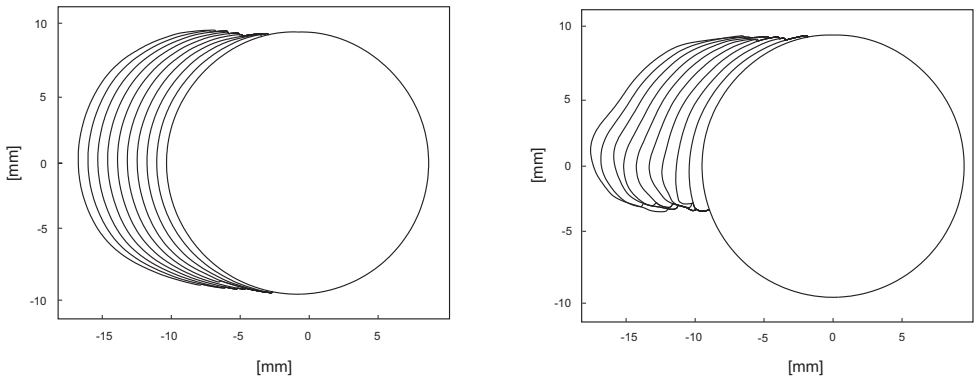

Figure 3: Ice accretion on an upstream (left) and downstream (right) cable with a cable spacing of 400mm. Icing conditions: wind velocity u=10 m/s, characteristic precipitation diameter MDV=75µm, air temperature T=−10°C, cable diameter d=349mm. The simulation had a duration of 10 minutes and a LCW = 1.0 g/m³

So far, the model does not account for wet ice growing conditions. Therefore a thermodynamic model will be implemented. Then, further studies should be performed to prove the model validity for

a broader range of meteorological conditions beyond the given examples of model verification. Also the relative movement of the individual conductors of the bundle is not considered. The shielding effect on the downstream cable can periodically vanish, when the cables are not in line due to cable oscillation. Different ice loading on the cables leads to deviating sag and thus changes the shielding affect.

ACKNOWLEDGMENT

The authors thankfully acknowledge the support of the German Research Foundation (DFG) given to the International Graduate School 802, Risk Management of Natural and Civilisation Hazards on Buildings and Infrastructure.

REFERENCES

Anderson, J. D., (1995). *Computational Fluid Dynamics*, McGraw-Hill

Bain, M., Gayet, J. F., (1982). "Contribution to the modeling of the ice accretion process: Ice density variation with the impact surface angle", Annals of Glaciology 4, 19-23

Bendel, W. B., Paton, D. (1981). "A review on the effect of ice storms on the power industry", Journal of Applied Meteorology 20, 1445-1449

Bundesnetzagentur für Elektrizität, Gas, Untersuchungsbericht Telekommunikation Post und Eisenbahnen, (2006). "Über die Versorgungsstörung im Netzgebiet des RWE im Münsterland vom 25.11.2005"

Comsol, (2007). Heat Transfer and Chemical Engineering Model User Guide for Comsol Multiphysics, COMSOL AB

Coulson, J. M., Richardson, J. F., (1991). *Particle Technology and Separation Processes*, Chemical Engineering, vol. 2, Butterworth-Heinemann

Diem, M., (1956). "Ice loads on high voltage conductors in the mountains", Archiv für Meteorologie, Geophysik und Bioklimatologi B7, 87-95

Franke, J., (2007). "Introduction to the prediction of wind effects on buildings by computational wind engineering (CWE) in Wind Effects on Buildings and Design of Wind-Sensitive Structures", *Wind Effects on Buildings and Design of Wind-Sensitive Structures*, 67-103

Fu, P., (2004). *Modelling and simulation of the ice accretion process on fixed or rotating cylindrical objects by boundary element method*, Ph.D., Thesis University of Quebec

Fu, P., Farzaneh, M., Bouchard, G., (2006). "Two-dimensional modelling of the ice accretion process on transmission line wires and conductors", Cold Regions Science and Technology 46, 132-146

Jones, K. F. (1998a). "An evaluation of the severity of the January 1998 ice storm in northern New England", Technical report for FEMA Region 1

Jones, K. F. (1998b). "A simple model for freezing rain ice loads", Atmospheric Research 46, 87-97

Kießling, F., Nefziger, P. & Kaintzyk, U., (2001). *Freileitungen: Planung, Berechnung, Ausführung*, Springer

Langmuir, I., Blodgett, K.B., (1946). "A Mathematical Investigation of Water Droplet Trajectories", AAF Technical Report 5418

Lämpke, D., (2006). Schadensanalyse an im Münsterland umgebrochenen Strommasten, Bundesanstalt für Materialforschung und Materialprüfung

Llinca, A., Llinca, F., Ignat, I., (1996). "Numerical study of iced conductors aerodynamics", *7th International Workshop on Atmospheric Icing of Structures*

Lozowski, E. P., Stallabrass, J. R., Hearty, P. F., (1983). "The icing of an unheated non-rotating cylinder Part 1: A simulation model", Journal of Climate and Applied Meteorology 22, 2053-2074

Macklin, W. C., (1962). "The density and structure of ice formed by accretion", Quarterly Journal of the Royal Meteorological Society, 88, 30-50

Makkonen, L., (1984). "Modelling of ice accretion on wires", Journal of Climate and Applied Meteorology 23, 929-939

Makkonen, L., (1989). "Estimation of wet snow accretion on structures", Cold Regions Science and Technology 17, 83-89

Makkonen, L., (1998). "Modeling power line icing in freezing precipitation", AtmosphericResearch 46,131-142

Makkonen, L., (2000). “Models for the growth of rime, glaze, icicles and wet snow on structures”, Phil. Trans. R. Soc. London 358, 2913-2939

Makkonen, L., Lozowski, E., (2005). “Fifty years of progress in modelling the accumulation of atmospheric ice on power network equipment”, *11th International Workshop on Atmospheric Icing of Structures*

Messinger, B. L., (1953). “Equilibrium temperature of an unheated icing surface as a function”, Journal of the Aeronautical Sciences 20, 29-41

Muhlerin, N. D., (1998). “Atmospheric icing and communication tower failure in the united states”, Cold Regions Science and Technology 27,91-104

Poots, G., (1996). *Ice and snow accretion on structures*, Research Studies Press LTD.

Schäfer, M., Turek, (1996). “Benchmark Computations of Laminar Flow Around a Cylinder”, *Flow Simulation with High-Performance Computers*, 52, 547-566

Schenk, O., Gärtner, K., (2004). “Solving Unsymmetric Sparse Systems of Linear Equations with PARDISO”, Journal of Future Generation Computer Systems, 20(3), 475-487

Schenk, O., Gärtner, K., (2006). “On fast factorization pivoting methods for symmetric indefinite systems”, Elec. Trans. Numer. Anal., 23, 158-179

Schlichting, H., Gersten K., (2006). *Grenzschicht-Theorie*, Springer

Waibel, K., (1956). “Die meteorologischen Bedingungen für Nebelfrostablagerungen an Hochspannungsleitungen im Gebirge”, Archiv für Meteorologie, Geophysik und Bioklimatologie B3, 74-83

Wilcox, D. C., (1998). *Turbulence modelling for CFD*, DCW Industries

Zienkiewicz, O. C., Taylor, R. L., Nithiaparsu, P. (2005). *The Finite Element Method for Fluid Dynamics*, Elsevier Butterworth-Heinemann